Terahertz All-Dielectric Magnetic Mirror Metasurfaces

Zhijie Ma,[†,‡,¶,§] Stephen M. Hanham,[‖] Pablo Albella,[¶] Binghao Ng,[§] Hsiao Tzu Lu,[⊥] Yandong Gong,[§] Stefan A. Maier,[*,¶] and Minghui Hong[*,‡]

†*NUS Graduate School for Integrative Sciences & Engineering (NGS), National University of Singapore, Singapore, 117456, Singapore*

‡*Department of Electrical and Computer Engineering, National University of Singapore, 117576, Singapore*

¶*Department of Physics, Imperial College London, London SW7 2AZ, UK*

§*Institute for Infocomm Research, A*STAR, 138632, Singapore*

‖*Department of Materials, Imperial College London, London SW7 2AZ, UK*

⊥*Data Storage Institute, A*STAR, 117608, Singapore*

E-mail: s.maier@imperial.ac.uk; elehmh@nus.edu.sg

Abstract

We demonstrate an all-dielectric metasurface operating in the terahertz band that is capable of engineering a reflected beam's spatial properties with high efficiency. The metasurface is formed from an array of silicon cube resonators which simultaneously support electric and magnetic dipolar Mie resonances. By controlling the interference between these modes, the amplitude and phase of a reflected wave can be arbitrarily controlled over a sub-wavelength area. We demonstrate the flexibility and utility of this metasurface by optimizing the surface to produce several reflected beam types including vortex and Bessel beams; the latter being useful for diffraction-free point-to-point

terahertz communications. Additionally, we show theoretically and experimentally how the metasurface can produce an all-dielectric magnetic mirror in the terahertz band.

Keywords

all-dielectric metamterials, metasurface, magnetic mirror, Mie resonance, terahertz, Bessel beam

Metasurfaces are the two dimensional counterpart of metamaterials[1] and allow the control of the phase, amplitude, and polarization of transmitted or reflected electromagnetic waves.[2] In the early stages of metamaterial and metasurface research, the magnetic response was engineered by artificial metallic split ring resonators (SRRs) that mimic a resonant LC circuit in which the circulating conduction current forms a magnetic dipole resonance.[3] One of the limitations of using metals at shorter wavelengths, particularly in the visible, is their large inherent Ohmic loss.[4] An alternate approach to metals is to use high-refractive index non-magnetic dielectric materials.[5–9] These materials can be appropriately structured so that they support distinct electric and magnetic dipole and higher-order Mie resonances, which can be employed to manipulate light-matter interaction and manifest exotic photonic behavior.[10,11]

Metasurfaces can introduce abrupt phase variations in incident waves by either the Pancharatnam-Berry phase method[12] or resonant phase retardation.[13] The Berry phase approach can be utilized only for circular polarization,[14,15] and due to the limited phase change range of π for Lorentzian resonators, a single resonance is not adequate for full 2π phase control of a scattered wave.[16] There are several methods commonly used to achieve the full 2π phase range. The first is to manipulate the phase of cross-polarized waves, however the theoretical maximum of power efficiency is limited to 25% for orthogonal polarization coupling.[17] Other methods include stacking multiple functional layers,[18–20] or operating in

reflection mode with a metal ground plane, with the disadvantage of being incompatible with many semiconductor industry processes.[21]

All-dielectric resonator metasurfaces provide another route for full range phase control by the simultaneous excitation of electric and magnetic dipoles. It has been proven analytically that a dielectric resonator with ideal electric and magnetic dipole modes can realize a perfect transmissive Huygens' surface.[22] In addition to this mechanism, high-efficiency all-dielectric metasurfaces have also been demonstrated by Lin et al utilizing the Pancharatnam-Berry phase, which is limited to circularly polarized light and the scattered wave is of opposite helicity.[15] Arbabi et al performed comprehensive studies on dielectric metasurfaces made from elliptical silicon posts which are considered as birefringent low-quality-factor Fabry-Perot resonators and different phase delay is introduced by the different effective refractive index. Such powerful control of phase and amplitude of the transmitted waves enables elaborate applications such as holograms and generation of cylindrical vector beams.[23]

In the applications of metasurfaces, the terahertz (THz) spectrum is of particular research interest due to its unique properties such as non-ionizing photon energy, spectral fingerprinting of inter-molecular vibrations, high transparency of certain optically opaque materials, making it highly desirable for applications in biological sensing, material analysis, and imaging.[24] This band is also promising for fast wireless communication due to the potentially large available spectrum. However, the prevalence of THz technologies has been impeded by the lack of compact high-power source and high-performance components.[25]

We design and fabricate an all-dielectric metasurface consisting of a periodic array of silicon cubes on a SiO_2 substrate that reflects THz electromagnetic waves by simultaneously exciting the electric and magnetic dipole modes with the characteristics of a magnetic mirror. The maximum electric field at the interface can strongly enhance the near-field light-matter interaction, enabling advances in biosensing, antennas, and THz optical components. A fabrication technique for realizing thick silicon resonators on an insulating substrate was devised specifically for the terahertz band. We also numerically show that by controlling

the geometry of the cube resonators, a phase tuning range of 2π with a near unity reflectivity can be obtained in reflection mode when the electric and magnetic dipole resonances overlap. We further demonstrate how this control over the reflected beam can be used to generate a number of different beam types. Specifically, these are an optical beam vortex and Bessel beam; both realized with high reflection efficiency by our single-layer all-dielectric metasurfaces.

Results and Discussion

We begin by considering a linearly polarized plane wave in the terahertz frequency range normally incident on an infinite array of high refractive index ($\epsilon_r = 11.7$) silicon cubes with negligible loss on a semi-infinite fused silica substrate ($n = 2$). The widths of the cube resonator are 150 μm in both the x and y directions, with height being 180 μm, and the lattice constants are 300 μm in both directions, as shown in the inset of Figure 1a. We used the commercial finite-difference-time-domain (FDTD) software Lumerical for the numerical simulations. The calculated reflection spectrum is shown as a dashed line in Figure 1a; a reflection peak of the amplitude 0.94 is observed at 0.48 THz, which is much higher than the normal Fresnel reflection from a planar silicon surface (R=0.3). Due to the symmetry of the individual cube and the array, the high-reflectance is invariant to the polarization state of the THz waves. The smaller reflection peaks at higher frequencies are due to the excitation of higher order modes and are not considered further here.

In Figure 1b, the scattering cross-section of a single isolated Si cube on a semi-infinite silica substrate is calculated to determine the spectral positions of the different multipolar contributions. According to Mie theory, any scattered field can be decomposed into the superposition of one or more eigenmodes, the most important being the magnetic and electric dipoles.[26] In most non-magnetic materials, the magnetic dipolar resonance is either not excited or poorly excited by a plane wave and is considered a dark mode. In our metasurface,

a magnetic dipolar resonance is supported by a circular displacement current, which has been shown to exist in high refractive-index dielectric structures.[10,27,28]

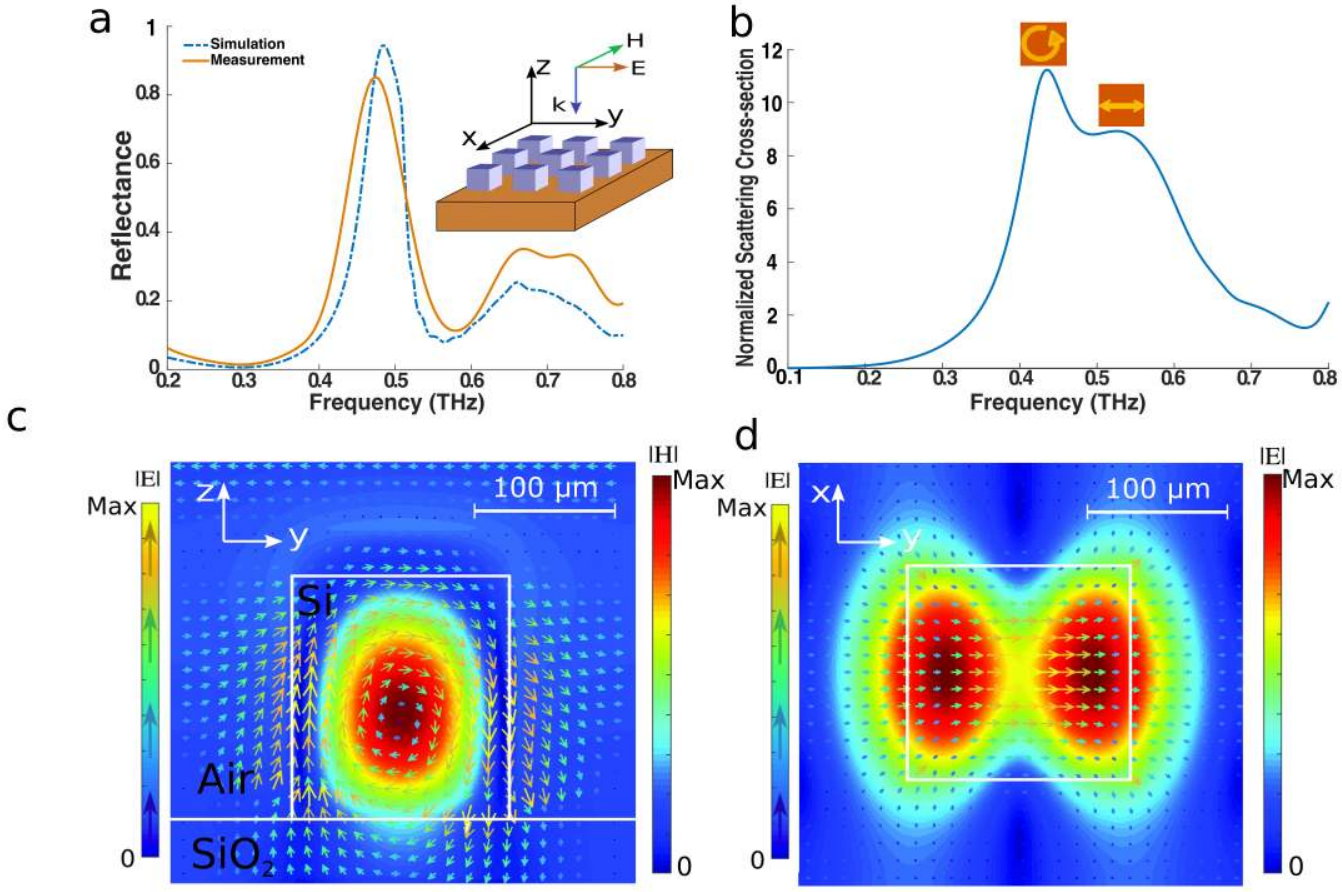

Figure 1: (a) Reflection spectra of the magnetic mirror. The inset shows a schematic of the structure with coordinate system and the polarization of the incident waves. (b) Normalized scattering cross-section of an individual (non-periodic) silicon cube on a silica substrate, with the two peaks corresponding to the electric and magnetic dipole resonances. (c) Electric and magnetic field distribution in the y-z plane at 0.48 THz. The magnetic dipole resonance is characterized by a magnetic field maximum in the center of the cube accompanied by a circulating electric field. (d) Electric field distribution in the x-y plane at 0.47 THz, showing the characteristic field of the electric dipole mode.

In the spectrum of Figure 1b, the first two peaks indicate the excitation of the lowest order magnetic dipole and electric dipole modes. The large normalized scattering cross-section indicates the strong coupling between the incident wave and the cube resonators. In the simulation of the periodic structure, the resonant frequencies of the electric and

magnetic modes are identified by their characteristic electric and magnetic fields. In a high-index resonator, when the size of the particle in the propagation direction is comparable to the effective wavelength in the dielectric material, the magnetic field of the incident wave can couple to the contra-directional circular displacement current associated with the magnetic dipole resonance mode, which is characterized by maximum magnetic field in the center of the particle, as shown in Figure 1c. A plot of the vector electric field in the y-z plane in Figure 1c shows the electric field circulating around the center of the cube, which also indicates that the magnetic dipole originates from the circular displacement current. The magnetic dipole generated by the electric circular displacement current is parallel to the magnetic field of the incident wave, giving a micro-cube of a non-magnetic material a non-unity effective permeability.[29] Figure 1d shows the electric field at 0.47 THz in the x-y plane when it is at its maximum value, with the vector electric field oriented in the direction of the incident wave's polarization, indicating the excitation of an electric dipole resonance. Also note that due to their spectral proximity, the electric field distribution of the electric dipole is also partially affected by the magnetic dipole mode.[30,31] The discrepancy in the spectral positions of the electric and magnetic dipole modes between the single particle and the periodic structure is attributed to the lattice interaction of the resonators[32] either through coupling or scattering. The electric and magnetic dipoles can be individually spectrally tuned by appropriately varying the micro-cubes geometric parameters[33] and the periodicities[34] in the transverse directions, so that the two modes can be tailored to overlap spectrally, suggesting that the electric and magnetic dipoles can be excited simultaneously.

The theory for the directional scattering of a single dielectric particles was first developed by Kerker[35] and has been experimentally demonstrated in the microwave[27] and visible regimes[36] with the two well-studied Kerker's conditions for full-forward and full-backward scattering.[37] However, these conditions only consider the coherent interference of the scattered fields from the electric and magnetic dipole resonances, while for a periodic metasurface structure the incident field must be considered as well.[21,22,38,39] In the periodic array case,

when the magnetic and electric dipoles are separated in frequency, if only one of the modes is excited individually, the field radiated from the single dipole is out of phase with the incident field, therefore, they interfere destructively in the forward direction, showing a perfect reflection peak, with distinct characteristic of a electric mirror and a magnetic mirror.[21,22,39] In the ideal situation when the two modes have exactly the same resonant frequency and damping factor, perfect transmission with arbitrary phase can be obtained.[22] In our study, by carefully engineering the geometry of the cube resonator and the periodicity, the two dipole modes can be brought close together in frequency to achieve a hybrid electric and magnetic mirror over a broad bandwidth. The simultaneous excitation of both modes enables the full 2π phase tuning range of the reflected waves, making an all-dielectric high-efficiency metasurface in reflection mode possible.

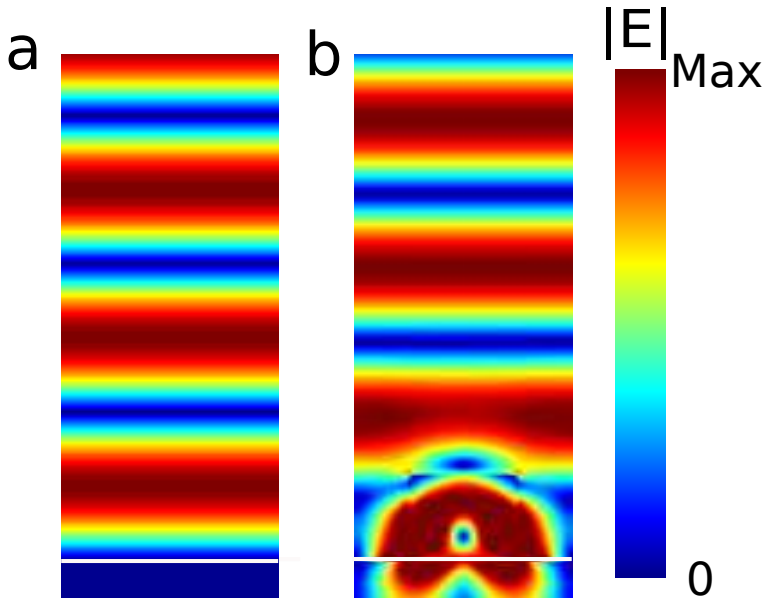

Figure 2: (a) Electric field magnitude of the standing wave formed by the interference of the incident wave and the reflected wave from a PEC. (b) Standing wave from the dielectric magnetic mirror.

When the cube resonators are arranged into a 2D array with a sub-wavelength periodicity, only the zeroth diffraction order is allowed to exist in free-space, creating plane waves normal to the surface in the far-field. In addition to the high reflection at the resonance frequency, we highlight that the metasurface has the characteristic of a magnetic mirror.

A perfect electric conductor (PEC) mirror has the boundary condition that the tangential electric field has to vanish at the interface, giving a π phase shift for the electric field of the reflected wave. The electric field node at the interface prohibits strong interaction of electromagnetic waves with sub-wavelength thickness analytes (or absorbers and emitters at shorter wavelengths) placed on the surface.To circumvent this limitation, various structures have been designed. Metallic metamaterial mirrors with subwavelength groove arrays have been demonstrated that achieve tunable phase reversal from 0 to π, corresponding to the cases of a pure magnetic mirror and electric mirror,[40] respectively. In a recently published work, Headland et al demonstrated a THz magnetic mirror using dielectric resonators on a gold film, in which high reflectivity is realized by the metal film while the magnetic dipole mode in the dielectric resonator antennas provide the desired phase shift. The employment of the metal film however introduces additional loss in the ground plane.[38] All-dielectric mirrors have been demonstrated using high-index tellurium (Te) cubes in the visible[41] and silicon in the infrared spectrum,[39] utilizing separate electric and magnetic dipole resonances to achieve either electric or magnetic mirror responses. Compared to the aforementioned methods, our design presents a realization of a magnetic mirror using low-loss all-dielectric structures with spectrally approaching electric and magnetic dipoles. The abrupt electric field phase change introduced by the excitation of the electric dipole resonance can be compensated by the phase change from the magnetic dipole resonance, leading to an overall zero phase shift with respect to the incident field, making a magnetic mirror. In Figure 2, we show the near-field responses of a perfect electric conductor (PEC) and the dielectric magnetic mirror. The comparison helps to demonstrate the phase delay difference. In Figure 2a, the standing wave of the electric field formed by the interference of the incident wave and the reflected wave vanishes at the interface due to the abrupt π phase change at the surface. While in Figure 2b, the standing wave pattern is $\lambda/4$ shifted compared to that of the PEC, with an electric field maximum at the interface, suggesting that the electric field of the reflected wave is in phase with the incident wave and experiences a zero degree

phase change. This is a characteristic of particular interest for THz sensing as the near-field interaction of the THz waves with analytes located on the surface is significantly enhanced so that the spectral signatures in the reflected waves can be utilized for identification; other applications include antennas[42] and THz electromagnetic components.

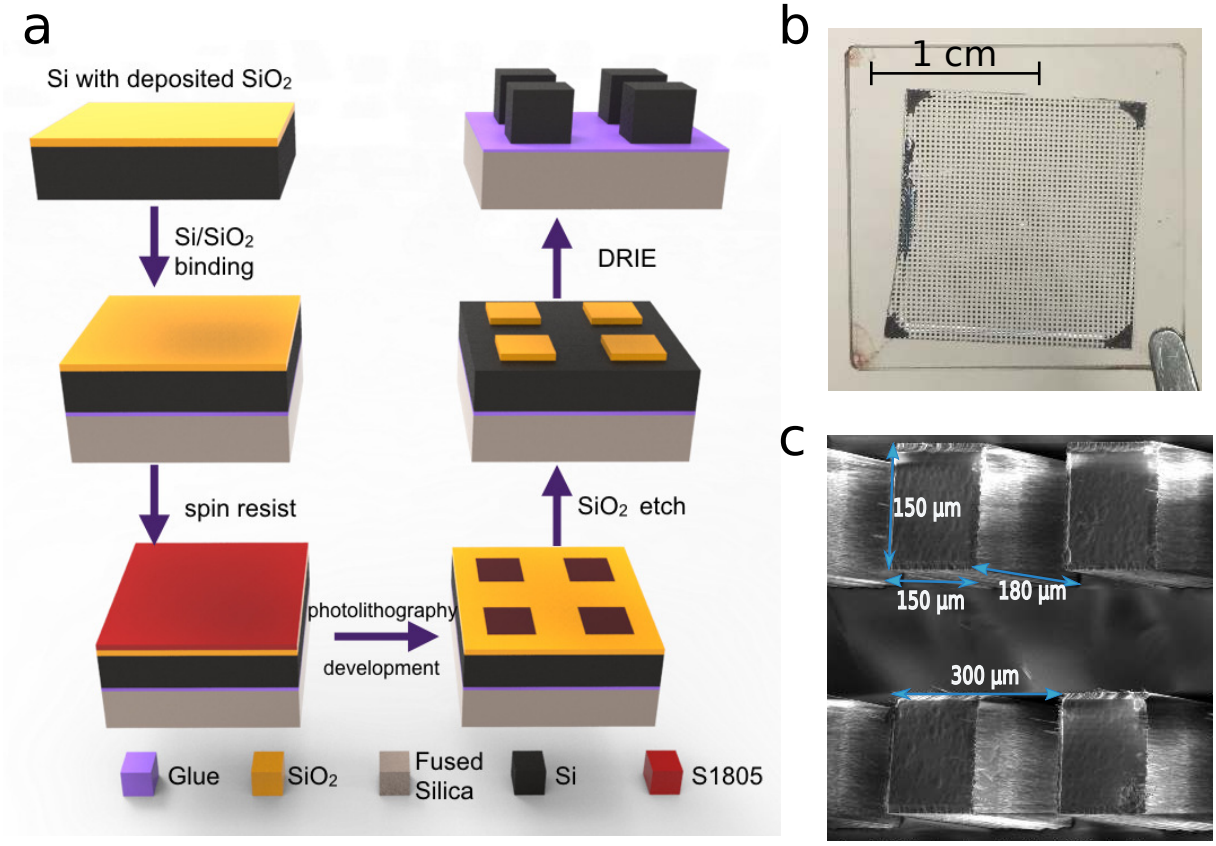

Figure 3: (a) Fabrication process of the silicon magnetic mirror. (b) A photo of the sample. (c) A SEM image of the fabricated Si magnetic mirror, with the geometry parameters shown.

The longer wavelength of THz waves requires an alternate fabrication process to that previously described for magnetic mirrors operating in the visible and IR spectrum.[39,41] In particular, the silicon on insulator(SOI) wafer cannot be grown by chemical vapour deposition (CVD), and the cube resonators cannot be fabricated by conventional one-step reactive ion etching because of the large thickness required for the silicon wafer. Therefore, we fabricated our samples by the process presented in Figure 3a. First, 500 nm SiO_2 is deposited on a

180 μm thick high-resistivity ($> 10,000$ Ω·cm) silicon wafer by inductively-coupled plasma chemical vapor deposition (ICP-CVD). The wafer is then directly bonded with a 2 mm fused silica substrate by a UV curable polymer optical adhesive spin-coated on it, followed by UV light exposure. High-resistivity silicon is widely used in THz optics due to its low loss and low dispersion over the THz spectrum. Conventional mask photolithography is employed to pattern the photoresist layer. The silicon wafer is etched by the Bosch deep reactive ion etching (DRIE) process (further details can be found in the Methods section). This process leaves an array of silicon micro-cubes attached to the fused silica substrate, as shown in Figure 3b. The SEM image in Figure 3c shows that each individual cube is 150 μm long both in the x- and y-directions, with a depth of 180 μm as designed. This direct fabrication route for achieving a thick silicon-on-insulator structure is simpler than other all-dielectric metasurfaces that need to be embedded in a homogenous low-index medium.[22,33,43] The reflection spectrum of the fabricated samples is obtained using a terahertz time-domain spectrometer (THz-TDS). A double-side polished high-resistivity silicon wafer is applied as a beam splitter. In the measured spectrum, a peak in the reflection amplitude of 0.85 is found at 0.48 THz, and the overall lineshape is in good agreement with the simulation result in Figure 1a. The lower reflection amplitude and the broadening of the peak in the experimental results are due to defects and inaccuracy of the sample fabrication.

All-Dielectric Reflective Metasurfaces

After the demonstration of the high reflectance of our structure, we proceed to the development of high-efficiency all-dielectric functional metasurfaces operating in reflection mode. In our structure, full 2π phase control is possible with the ability to stimulate both the electric and magnetic dipole resonances simultaneously in the high refractive index dielectric resonator by varying the geometries of the silicon cube resonators in the transverse x and y directions. This principle has been successfully applied to dielectric metasurfaces in

transmission mode when the electric and magnetic dipole modes overlap, and proven to be applicable for ultra-thin lenses and optical vortex beam conversion in the near-infrared spectrum.[21] A complementary all-dielectric metasurface in reflection mode is highly desirable for certain applications and it has the advantage of avoiding the reflection loss at the exiting interface and the Fabry-Perot modes in the substrate. In this section, we demonstrate numerically, to the best of our knowledge, the first all-dielectric metasurfaces operating in reflection mode for linearly polarized waves. The high-efficiency metasurfaces with full phase tuning range in reflection mode are achieved by bringing close the two reflection peaks of electric and magnetic dipole resonances.

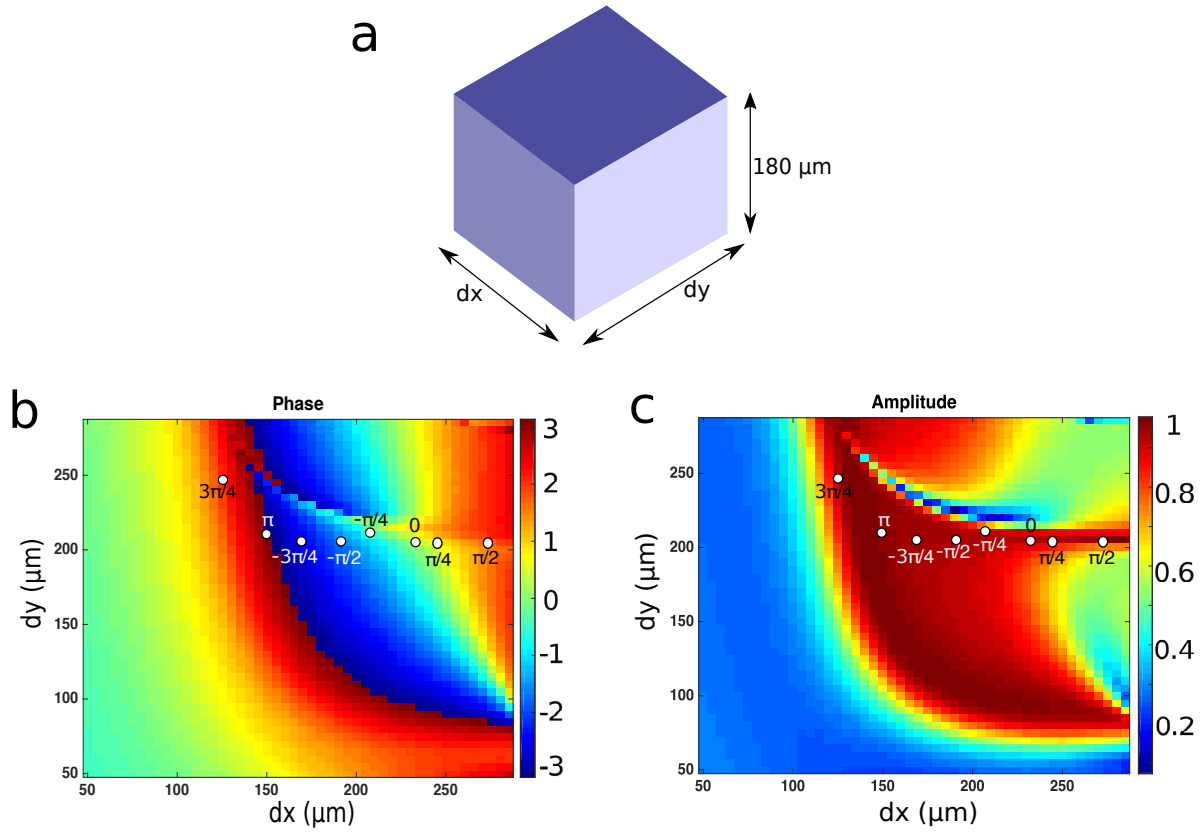

Figure 4: (a) Schematic of the silicon cube resonator on a glass substrate, with the height fixed as 180 μm. (b) Phase and (c) amplitude of the back-scattered wave with varying dimensions in x- and y-directions.

In the FDTD simulation, we fix the thickness of the micro-cube to be 180 μm and change the dimensions of the cubes in x and y directions, while keeping the periodicity constant

at 300 μm. The phase and amplitude of the reflected waves are calculated as a function of the geometries of the silicon cubes along the x- and y- directions. The results are shown in Figures 4b and 4c. It can be seen that the full phase coverage from 0 to 2π can be achieved while maintaining a high efficiency of reflection larger than 0.9. Eight building blocks of different geometries with a phase increment of $\pi/4$ and constant reflectance larger than 0.9 are selected. Figure 4 can serve as a dataset for the design of various functional metasurfaces with given phase and amplitude reflection spatial distributions.

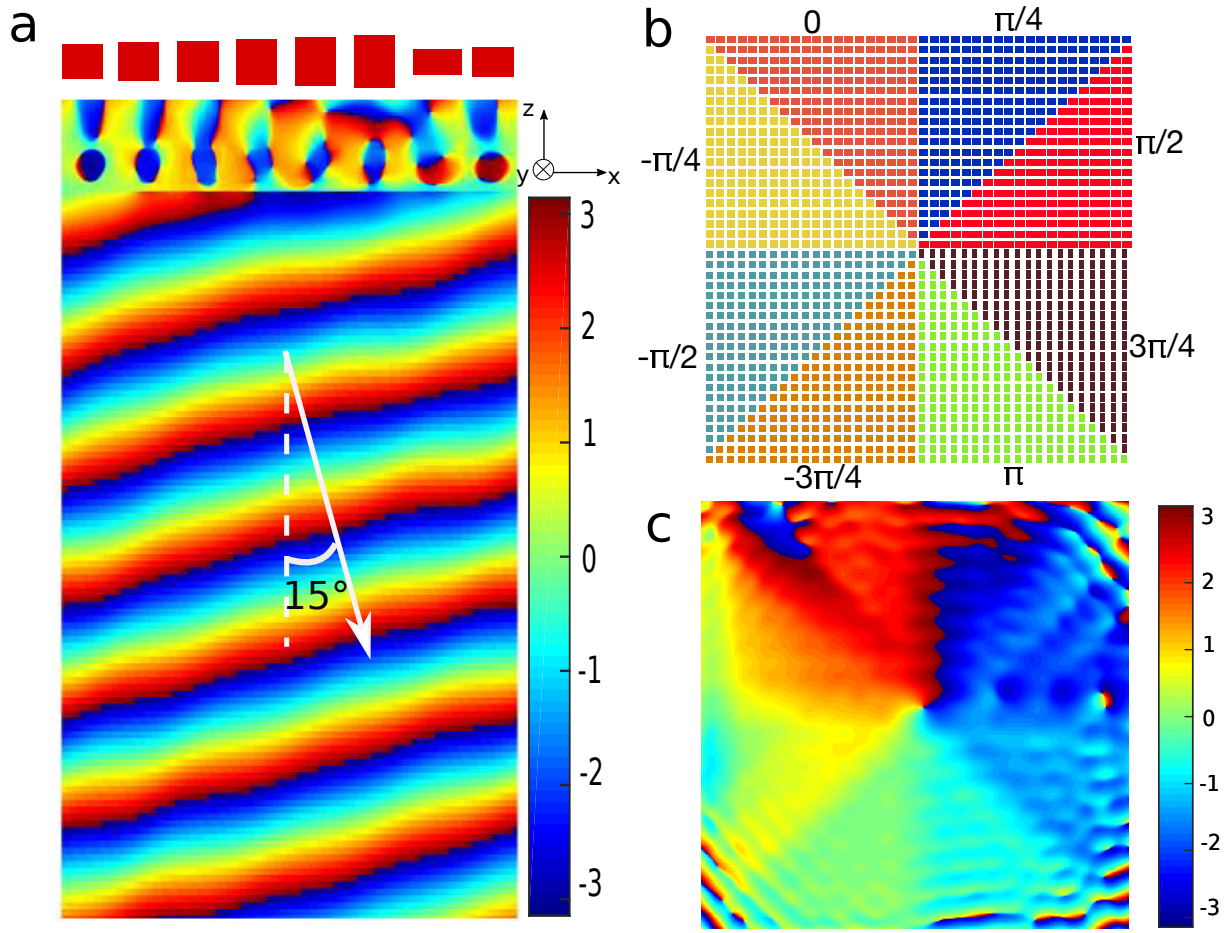

Figure 5: (a) Schematic of the eight micro-blocks and the simulated phase of the reflected wave. (b) Schematic of the vortex beam converter with eight sectors covering the phase space from 0 to 2π with $\pi/4$ increments. (c) Generated wave with vortical phase variation.

As a proof of concept, we first demonstrate a metasurface to achieve anomalous reflection. As shown in Figure 5a, a normally incident wave can be transformed to a reflected wave with a tilted wavefront by varying the phase of the reflected wave along the x-direction when a

y-polarized wave is incident. Eight building blocks of different dimensions which introduce a gradient phase increment of $\pi/4$ are arranged accordingly along the x-direction, with the periodicity being fixed at 300 μm in both x- and y-directions, the supercell $a = 2400$ μm along the x-direction, and the target wavelength $\lambda = 620$ μm (0.48 THz). The resultant reflected wave has an anomalous angle of 15° as determined by

$$sin(\alpha) = \lambda/a \tag{1}$$

with a high reflectance of 0.75. The anomalous reflection angle can be customised by controlling the phase elements distribution and distances.

To further demonstrate the capability of the metasurface to manipulate the reflected phase, we designed a phase-gradient spatial light modulator that can convert an incident homogeneous Gaussian beam into a beam with first-order vortical phase variation. An optical vortex beam with orbital angular momentum shows great promises in quantum information processing, multiplexing communication, and optical torque at nanoscale.[44,45] To achieve this goal, we patterned the eight building micro-blocks with different phases into the eight sectors incrementally, as in Figure 5b, the device contains 40 unit cells in both x- and y-directions, with the area being 12 mm × 12 mm. In the simulations a monitor was positioned $\sim \lambda$ behind the incident source plane to record the energy and phase information of the reflected waves. The resultant reflected wave phase in Figure 5c has a clear vortical phase variation, and the power efficiency of the reflected wave is larger than 80% of the incident wave.

Bessel beams are diffraction-free solutions to Maxwell's equations in free-space with the characteristics of a non-spreading central maxima and self-healing along the propagation direction.[46] An ideal Bessel beam has the mathematical expression:

$$E(r, \phi, z) = A_0 exp(ik_z z) J_n(k_r r) exp(\pm in\phi) \tag{2}$$

where k_z and k_r are the wavevectors in the propagation and radial directions, respectively,

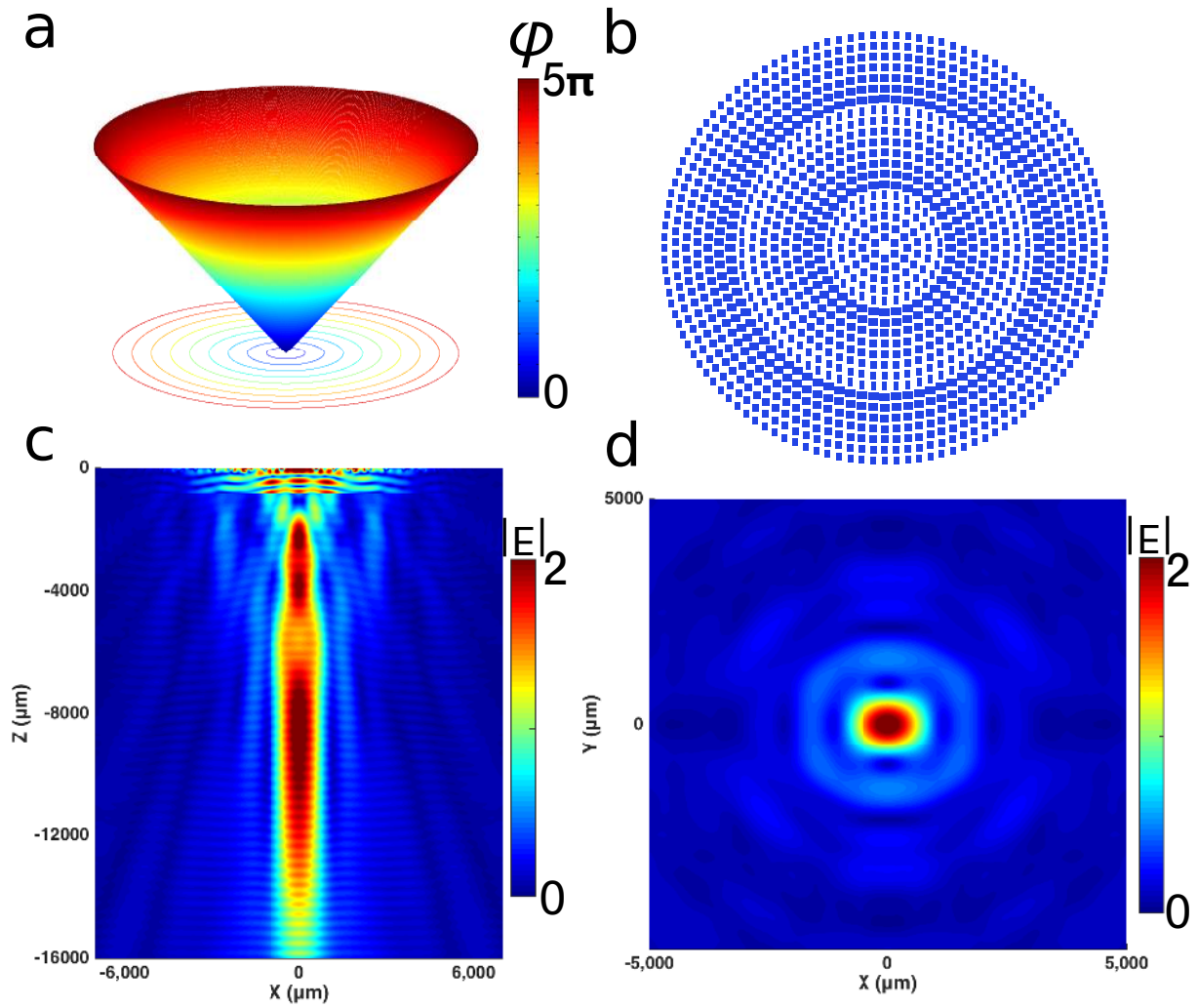

Figure 6: (a) Phase variation needed for the generation of a Bessel beam. (b) Schematic of the Bessel beamformer with 20 concentric rings of micro-blocks with $\pi/4$ phase increment. (c) Side view of the electric field distribution of the generated Bessel beam. (d) Cross-section view of the electric field distribution of the Bessel beam.

and J_n is the $n-th$ order Bessel function. A Bessel beam is essentially a ring in Fourier space. Due to the infinite energy in a theoretical Bessel beam, only an approximation can be achieved in practice. Common methods to create Bessel beams include using axicon lenses or by filtering through a ring in the back focal plane.[47] These are bulky and incompatible with on-chip integration. With the emergence of metasurfaces Bessel beams can also be generated by spatially varying the phase response of each scattering unit cell.[48] The phase profile of a Bessel beam is designed to be linear from the center of the metasurface as shown in Figure 6a according to:

$$\varphi_A(x,y) = \frac{2\pi}{\lambda}\sqrt{x^2+y^2}\sin\beta \tag{3}$$

The same building blocks taken from Figure 4 are arranged into 20 concentric rings with linear phase increments of $\pi/4$, with the same periodicity of 300 μm as in Figure 6b, and a phase increase from 0 to 5π. The resultant reflected wave in Figure 6c shows a constant high-intensity E-field along the propagation direction, with a focal depth longer than 27λ, and the E-field in the cross-section shows a Bessel distribution. The long focal depth and diffractionless nature of Bessel beams has great potential for THz point-to-point wireless communications. The focus length can be further improved with a larger aperture size, or with a less steep phase variation.

Conclusions

In summary, we have demonstrated both numerically and experimentally a high-efficiency all-dielectric single-layer metasurface which operates in reflection mode with the characteristics of a magnetic mirror in the THz band. The all-dielectric magnetic mirror design is polarization independent and polarization preserving, and can be scaled to operate in other bands of the electromagnetic spectrum. The metasurface consists of periodic silicon micro-cubes on a silica substrate which support both electric and magnetic dipole resonances in the same frequency range. By controlling the geometry of the micro-cube resonators the

interaction of the dipole resonances can be manipulated and the phase of a reflected wave can be tailored from 0 to 2π while maintaining a high reflectivity. We demonstrated that the metasurface is useful for the generation of several reflected beam types and phenomena: anomalous surface reflection, optical vortex beams and Bessel beams, which have potential application for THz communications. A micro-fabrication process was developed for creating the thick silicon structures on an insulator substrate, and it can be applied for the fabrication of the other metasurfaces we proposed. The all-dielectric metasurface is a promising alternative to metallic structures for its low dissipative loss and compatibility with the semiconductor industry.

Methods

Microfabrication of Sample: 500 nm SiO_2 is deposited on the 180 μm thick high-resistivity ($> 10,000\ \Omega{\cdot}cm$) silicon wafer by inductively-coupled plasma chemical vapor deposition (ICP-CVD). The thickness of the SiO_2 layer is decided by the selectivity of the etching gas ions on Si and SiO_2. The wafer is then directly bonded on a 2 mm fused silica substrate with a thin layer of spin-coated UV curable polymer optical adhesive (Norland Optical Adhesive 85) and 20 minutes of UV light exposure (2.5 W/cm^2). The pattern of square array is formed by conventional mask photolithography on SiO_2 with a 500 nm layer of S1805 photoresist. The SiO_2 layer at open area is then removed by C_4F_8 gas and the remaining pattern is kept as a protection mask for subsequent etching. The silicon wafer is etched by the Bosch process using deep reactive ion etching technique (DRIE; SPTS ADE). Each cycle of the Bosch process consists of 5 s of deposition and 15 s of etching. In the deposition step, the C_4F_8 gas (85 sccm) is utilized with 600 W ICP power in 35 mTorr pressure. In the etching step, a mixture of SF_6 (130 sccm) and O_2 (13 sccm) is applied with 600 W ICP power and 30 W bias power, in 35 mTorr pressure. This process cycle is then repeated till the silicon is completely removed. Solid silicon micro-cube arrays are kept attached to

the fused silica substrate as shown in Figure 1b. The SEM image in Figure 1c shows that the individual cube is 150 μm along both the x- and y-directions, at the depth of 180 μm as designed. The periodicities in x- and y-directions are both 300 μm. This direct fabrication route for a thick silicon-on-insulator structure relaxed the fabrication requirements compared with most all-dielectric metasurfaces that need to be embedded in a homogenous medium.

THz-TDS characterization: the Menlo Tera K15 fiber-coupled terahertz time domain spectrometer (THz-TDS) is used in a reflection geometry as shown in Figure 7. A double-side polished high-resistivity ($> 10,000\ \Omega{\cdot}cm$) silicon wafer is applied as a beam splitter for THz waves. An iris with the diameter of 10 mm is set in front of the sample or mirror to isolate the THz waves reflected from the patterned area, and the measured reflectance of the sample is normalized to a silver mirror with the same iris diameter. All measurements are performed in atmosphere. The characterization system is compact with the total optical length less than 30 cm. The collected data is in the time-domain and by application of the Fast Fourier Transform (FFT) we can obtain the reflection spectrum.

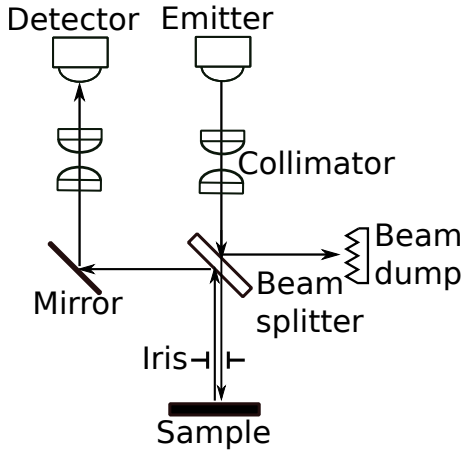

Figure 7: The optical path for the THz-TDS measurement setup.

Acknowledgement

Z. Ma acknowledges the National University of Singapore Graduate School for Integrative Sciences and Engineering (NGS) scholarship. This research is supported by the Na-

tional Research Foundation, Prime Minister's Office, Singapore under its Competitive Research Program (CRP Award No. NRF-CRP10-2012-04), and partially supported by SERC A*STAR, Singapore under project No.1420200044, and EDB, Singapore grant No. S15-1322-IAF OSTIn-SIAG. S. A. M acknowledges the Royal Society, the Leverhulme Trust, and the Lee-Lucas Chair for funding.

References

(1) Zheludev, N. I.; Kivshar, Y. S. From metamaterials to metadevices. *Nat. Mater.* **2012**, *11*, 917–924.

(2) Kildishev, A. V.; Boltasseva, A.; Shalaev, V. M. Planar Photonics with Metasurfaces. *Science* **2013**, *339(6125)*, 1232009.

(3) Pendry, J. B.; Holden, a. J.; Robbins, D. J.; Stewart, W. J. Magnetism from conductors and enhanced nonlinear phenomena. *IEEE Trans. Microwave Theory Tech.* **1999**, *47*, 2075–2084.

(4) Khurgin, J. B. How to deal with the loss in plasmonics and metamaterials. *Nat. Nanotechnol.* **2015**, *10*, 2–6.

(5) Yang, Y.; Wang, W.; Moitra, P.; Kravchenko, I. I.; Briggs, D. P.; Valentine, J. Dielectric Meta-Reflectarray for Broadband Linear Polarization Conversion and Optical Vortex Generation. *Nano Lett.* **2014**, *14*, 1394–1399.

(6) Yang, Y.; Kravchenko, I. I.; Briggs, D. P.; Valentine, J. All-dielectric metasurface analogue of electromagnetically induced transparency. *Nat. Commun.* **2014**, *5*, 5753.

(7) Bakker, R. M.; Permyakov, D.; Yu, Y. F.; Markovich, D.; Paniagua-Domínguez, R.; Gonzaga, L.; Samusev, A.; Kivshar, Y. S.; Luk'yanchuk, B.; Kuznetsov, A. I. Magnetic and Electric Hotspots with Silicon Nanodimers. *Nano Lett.* **2015**, *15*, 2137–2142.

(8) Hopkins, B.; Filonov, D. S.; Miroshnichenko, A. E.; Monticone, F.; Alù, A.; Kivshar, Y. S. Interplay of Magnetic Responses in All-Dielectric Oligomers To Realize Magnetic Fano Resonances. *ACS Photonics* **2015**, *2*, 724–729.

(9) Basharin, A. A.; Kafesaki, M.; Economou, E. N.; Soukoulis, C. M.; Fedotov, V. a.; Savinov, V.; Zheludev, N. I. Dielectric Metamaterials with Toroidal Dipolar Response. *Phys. Rev. X* **2014**, *5*, 011036.

(10) Zhao, Q.; Zhou, J.; Zhang, F.; Lippens, D. Mie resonance-based dielectric metamaterials. *Mater. Today* **2009**, *12*, 60–69.

(11) Jahani, S.; Jacob, Z. All-dielectric metamaterials. *Nat. Nanotechnol.* **2016**, *11*, 23–36.

(12) Huang, L.; Chen, X.; Muhlenbernd, H.; Li, G.; Bai, B.; Tan, Q.; Jin, G.; Zentgraf, T.; Zhang, S. Dispersionless Phase Discontinuities for Controlling Light Propagation. *Nano Lett.* **2012**, *12*, 5750–5755.

(13) Yu, N.; Genevet, P.; Kats, M. A.; Aieta, F.; Tetienne, J.-P.; Capasso, F.; Gaburro, Z. Light Propagation with Phase Reflection and Refraction: Generalized Laws of Reflection and Refraction. *Science* **2011**, *334.6054*, 333–337.

(14) Kim, M.; Wong, A. M.; Eleftheriades, G. V. Optical Huygens' Metasurfaces with Independent Control of the Magnitude and Phase of the Local Reflection Coefficients. *Phys. Rev. X* **2014**, *4*, 041042.

(15) Lin, D.; Fan, P.; Hasman, E.; Brongersma, M. L. Dielectric gradient metasurface optical elements. *Science* **2014**, *345*, 298–302.

(16) Pors, A.; Bozhevolnyi, S. I. Plasmonic metasurfaces for efficient phase control in reflection. *Opt. Express* **2013**, *21*, 27438.

(17) Arbabi, A.; Faraon, A. Fundamental limits of ultrathin metasurfaces. *Preprint at http://arXiv.org/abs/1411.2537* **2014**,

(18) Pfeiffer, C.; Emani, N. K.; Shaltout, A. M.; Boltasseva, A.; Shalaev, V. M.; Grbic, A. Efficient light bending with isotropic metamaterial Huygens' surfaces. *Nano Lett.* **2014**, *14*, 2491–2497.

(19) Zhao, Y.; Belkin, M.; Alù, A. Twisted optical metamaterials for planarized ultrathin broadband circular polarizers. *Nat. Commun.* **2012**, *3*, 870.

(20) Monticone, F.; Estakhri, N. M.; Alù, A. Full Control of Nanoscale Optical Transmission with a Composite Metascreen. *Phys. Rev. Lett.* **2013**, *110*, 203903.

(21) Shalaev, M. I.; Sun, J.; Tsukernik, A.; Pandey, A.; Nikolskiy, K.; Litchinitser, N. M. High-Efficiency All-Dielectric Metasurfaces for Ultracompact Beam Manipulation in Transmission Mode. *Nano Lett.* **2015**, *15*, 6261–6266.

(22) Decker, M.; Staude, I.; Falkner, M.; Dominguez, J.; Neshev, D. N.; Brener, I.; Pertsch, T.; Kivshar, Y. S. High-Efficiency Dielectric Huygens' Surfaces. *Adv. Opt. Mater.* **2015**, *3*, 813–820.

(23) Arbabi, A.; Horie, Y.; Bagheri, M.; Faraon, A. Dielectric metasurfaces for complete control of phase and polarization with subwavelength spatial resolution and high transmission. *Nat. Nanotechnol.* **2015**, *10*, 937–943.

(24) Tonouchi, M. Cutting-edge terahertz technology. *Nat. Photonics* **2007**, *1*, 97–105.

(25) Mittleman, D. M. Frontiers in terahertz sources and plasmonics. *Nat. Photonics* **2013**, *7*, 666–669.

(26) Bohren, C. F.; Huffman, D. R. *Absorption and scattering of light by small particles*; John Wiley & Sons, 2008.

(27) Geffrin, J. M.; García-Cámara, B.; Gómez-Medina, R.; Albella, P.; Froufe-Pérez, L. S.; Eyraud, C.; Litman, A.; Vaillon, R.; González, F.; Nieto-Vesperinas, M.; Sáenz, J. J.;

Moreno, F. Magnetic and electric coherence in forward- and back-scattered electromagnetic waves by a single dielectric subwavelength sphere. *Nat. Commun.* **2012**, *3*, 1171.

(28) Kuznetsov, A. I.; Miroshnichenko, A. E.; Fu, Y. H.; Zhang, J.; Luk'yanchuk, B. Magnetic light. *Sci. Rep.* **2012**, *2*, 492.

(29) Ahmadi, A.; Mosallaei, H. Physical configuration and performance modeling of all-dielectric metamaterials. *Phys. Rev. B: Condens. Matter Mater. Phys.* **2008**, *77*, 1–11.

(30) Albella, P.; Poyli, M. A.; Schmidt, M. K.; Maier, S. a.; Moreno, F.; Sáenz, J. J.; Aizpurua, J. Low-loss electric and magnetic field-enhanced spectroscopy with subwavelength silicon dimers. *J. Phys. Chem. C* **2013**, *117*, 13573–13584.

(31) Albella, P.; Shibanuma, T.; Maier, S. A. Switchable directional scattering of electromagnetic radiation with subwavelength asymmetric silicon dimers. *Sci. Rep.* **2015**, *5*, 18322.

(32) Ng, B.; Hanham, S. M.; Giannini, V.; Chen, Z. C.; Tang, M.; Liew, Y. F.; Klein, N.; Hong, M. H.; Maier, S. a. Lattice resonances in antenna arrays for liquid sensing in the terahertz regime. *Opt. Express* **2011**, *19*, 14653.

(33) Staude, I.; Miroshnichenko, A. E.; Decker, M.; Fofang, N. T.; Liu, S.; Gonzales, E.; Dominguez, J.; Luk, T. S.; Neshev, D. N.; Brener, I. Tailoring directional scattering through magnetic and electric resonances in subwavelength silicon nanodisks. *ACS Nano* **2013**, *7*, 7824–7832.

(34) Wang, F.; Wei, Q.-H.; Htoon, H. Generation of steep phase anisotropy with zero-backscattering by arrays of coupled dielectric nano-resonators. *Appl. Phys. Lett.* **2014**, *105*, 121112.

(35) M. Kerker and C. L. Giles, D.-S. W. Electromagnetic scattering by magnetic spheres. *Opt. Express* **1983**, *73*, 765–767.

(36) Fu, Y. H.; Kuznetsov, A. I.; Miroshnichenko, A. E.; Yu, Y. F.; Luk'yanchuk, B. Directional visible light scattering by silicon nanoparticles. *Nat. Commun.* **2013**, *4*, 1527.

(37) Nieto-Vesperinas, M.; Gomez-Medina, R.; Saenz, J. J. Angle-suppressed scattering and optical forces on submicrometer dielectric particles. *J. Opt. Soc. Am. A* **2011**, *28*, 54–60.

(38) Headland, D.; Nirantar, S.; Withayachumnankul, W.; Gutruf, P.; Abbott, D.; Bhaskaran, M.; Fumeaux, C.; Sriram, S. Terahertz Magnetic Mirror Realized with Dielectric Resonator Antennas. *Adv. Mater.* **2015**, *27*, 7137–7144.

(39) Moitra, P.; Slovick, B. a.; Li, W.; Kravchenko, I. I.; Briggs, D. P.; Krishnamurthy, S.; Valentine, J. Large-Scale All-Dielectric Metamaterial Perfect Reflectors. *ACS Photonics* **2015**, *2*, 692–698.

(40) Esfandyarpour, M.; Garnett, E. C.; Cui, Y.; McGehee, M. D.; Brongersma, M. L. Metamaterial mirrors in optoelectronic devices. *Nat. Nanotechnol.* **2014**, *9*.

(41) Liu, S.; Sinclair, M. B.; Mahony, T. S.; Jun, Y. C.; Ginn, J.; Bender, D. A.; Wendt, J. R.; Ihlefeld, J. F.; Clem, P. G.; Wright, J. B.; Brener, I. Optical magnetic mirrors without metals. *Optica* **2014**, *1*, 250–256.

(42) Feresidis, A. P.; Goussetis, G.; Wang, S.; Vardaxoglou, J. C. Artificial magnetic conductor surfaces and their application to low-profile high-gain planar antennas. *IEEE Trans. Antennas Propag.* **2005**, *53*, 209–215.

(43) Saurtter, J.; Staude, I.; Decker, M.; Rusak, E.; Neshev, D. N.; Brener, I.; Kivshar, Y. S. Active Tuning of All-Dielectric Metasurfaces. *ACS Nano* **2015**, *9*, 4308–4315.

(44) Genevet, P.; Yu, N.; Aieta, F.; Lin, J.; Kats, M. a.; Blanchard, R.; Scully, M. O.; Gaburro, Z.; Capasso, F. Ultra-thin plasmonic optical vortex plate based on phase discontinuities. *Appl. Phys. Lett.* **2012**, *100*, 2012–2014.

(45) Wang, J.; Yang, J.-Y.; Fazal, I. M.; Ahmed, N.; Yan, Y.; Huang, H.; Ren, Y.; Yue, Y.; Dolinar, S.; Tur, M.; Willner, A. E. Terabit free-space data transmission employing orbital angular momentum multiplexing. *Nat. Photonics* **2012**, *6*, 488–496.

(46) Durnin, J.; Miceli, J.; Eberly, J. H. Diffraction-free beams. *Phys. Rev. Lett.* **1987**, *58*, 1499–1501.

(47) McGloin, D.; Dholakia, K. Bessel beams: diffraction in a new light. *Contemp. Phys.* **2005**, *46*, 15–28.

(48) Aieta, F.; Genevet, P.; Kats, M. a.; Yu, N.; Blanchard, R.; Gaburro, Z.; Capasso, F. Aberration-free ultrathin flat lenses and axicons at telecom wavelengths based on plasmonic metasurfaces. *Nano Lett.* **2012**, *12*, 4932–4936.

For Table of Contents Use Only

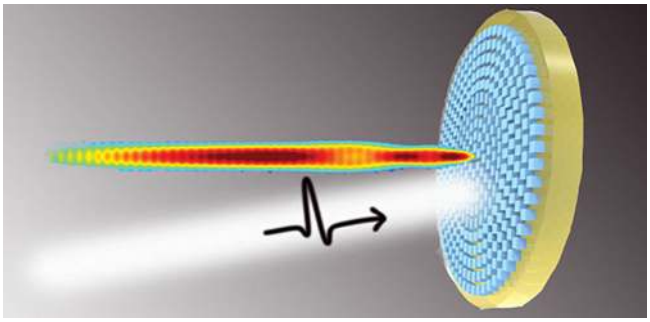

Figure 8: For Table of Contents Only

Title: Terahertz All-Dielectric Magnetic Mirror Metasurfaces

Authors: Zhijie Ma, Stephen M. Hanham, Pablo Albella, Binghao Ng, Lu Hsiao Tzu, Yandong Gong, Stefan A. Maier, and Minghui Hong